Journal of Physics and Chemistry of Solids 71 (2010) 1131–1136

Contents lists available at ScienceDirect

Journal of Physics and Chemistry of Solids

journal homepage: www.elsevier.com/locate/jpcs

Electrochemical deposition of Bi_2Te_3-based thin films

Liqin Qiu [a], Jian Zhou [a,*], Xuan Cheng [a,b,*], Rajeev Ahuja [c]

[a] Department of Materials Science and Engineering, College of Materials, Xiamen University, Xiamen, Fujian 361005, China
[b] Fujian Key Laboratory of Advanced Materials, Xiamen University, Xiamen, Fujian 361005, China
[c] Department of Physics and Materials Science, Condensed Matter Theory Group, Uppsala University, Box 530, 75121 Uppsala, Sweden

ARTICLE INFO

Keywords:
A. Chalcogenides
B. Crystal growth
C. Electron microscopy
D. Microstructure

ABSTRACT

The electrochemical reduction processes on stainless-steel substrates from an aqueous electrolyte composed of nitric acid, Bi^{3+}, $HTeO_2^+$, SbO^+ and H_2SeO_3 systems were investigated using cyclic voltammetry. The thin films with a stoichiometry of Bi_2Te_3, $Bi_{0.5}Sb_{1.5}Te_3$ and $Bi_2Te_{2.7}Se_{0.3}$ have been prepared by electrochemical deposition at selected potentials. The structure, composition, and morphology of the films were studied by X-ray diffraction (XRD), environmental scanning electron microscopy (ESEM) and electron microprobe analysis (EMPA). The results showed that the films were single phase with the rhombohedral Bi_2Te_3 structure. The morphology and growth orientation of the films were dependent on the deposition potentials.

1. Introduction

Bismuth telluride and its derivative compounds have proven to be one of the best thermoelectric materials with the highest figure of merit for thermoelectric (TE) applications at room temperature such as thermoelectric generators [1] and coolers [2]. They are traditionally synthesized by powder metallurgy [3] and zone melting processes [4] in bulk forms. Requirements of miniaturization for TE devices stimulate the research on fabricating Bi_2Te_3-based thin films by sputtering and evaporation methods [5–6]. However, those techniques are expensive and not readily to produce large-area TE materials. Electrochemical deposition may provide an alternative process to those methods. Moreover, it is easy to adjust the composition and the thickness of the deposit by changing the electrodepositing parameters.

So far, many studies have been devoted to the fabrication of Bi_2Te_3 [7–9] thin films. The p-type $Bi_{0.5}Sb_{1.5}Te_3$ [10–12] and n-type $Bi_2Te_{2.7}Se_{0.3}$ [13–15] have also attracted wide attention recently for their better thermoelectric properties. There have been studied on the electrochemical deposition of Bi_2Te_3 and its derivative compounds on different substrates such as Au [16], Pt [17], Ti [18] and gold sputtered-aluminum [8,19,20] These substrates are expensive or obtained by complicated technology for all of which are not suitable for practical applications of the TE materials. Stainless-steel may become a candidate for its cheap and wide source. However, few researches concerning the fabrication of Bi_2Te_3 films on stainless-steel substrates [21] have been carried out.

In this work, the reductive processes of Bi–Te binary system, Bi–Sb–Te and Bi–Te–Se ternary systems on the stainless-steel electrode were systematically studied using cyclic voltammetry. The stoichiometric Bi_2Te_3, $Bi_{0.5}Sb_{1.5}Te_3$ and $Bi_2Te_{2.7}Se_{0.3}$ thin films were obtained by electrochemical deposition at selected potentials.

2. Experimental section

The solutions were obtained, respectively, by dissolution of $Bi(NO_3)_3 \cdot 5H_2O$, TeO_2, Sb_2O_3 and SeO_2 in concentrated nitric acid (65%). In order to achieve higher solubility of Sb_2O_3, tartaric acid was used as a complexing reagent added into the solutions with Sb. All the chemical agents are analytical grade. A conventional three-electrode cell was used for the deposition of Bi_2Te_3-based thin films with the Pt foil (9 cm^2) as the counter electrode and saturated calomel electrode (SCE) as the reference electrode. Stainless-steel (1 cm × 1 cm) was chosen as substrate (the working electrode). The substrates were degreased by acetone, rinsed with distilled water, treated with ethanol and subsequently dried in the air. The films were electrochemically deposited onto stainless-steel at the selected potentials for 30 min. Then the films were removed from the electrolytes and treated in three steps: dipped in HNO_3 (pH=1) solution for 1 min, rinsed with ethanol and distilled water, and followed by drying in air.

The compositions were obtained by electron microprobe analysis (JEOL JXA-8100, EMPA), the surface morphologies were studied by environmental scanning electron microscope

* Corresponding authors. Tel.: +86 592 218 6664; fax: +86 592 2183937.
E-mail addresses: jzhou@xmu.edu.cn (J. Zhou), xcheng@xmu.edu.cn (X. Cheng).

0022-3697/$ - see front matter © 2010 Elsevier Ltd. All rights reserved.
doi:10.1016/j.jpcs.2010.03.020

(FEI XL30, ESEM) and the structures of the films were investigated by X-ray diffraction (X′ pert PRO, XRD).

3. Results and discussion

3.1. Cyclic voltammetry analysis

Cyclic voltammetry (CV) was used to find the appropriate potential range for deposition, then the films were deposited at the selected potentials. The following summarize the electrochemical behaviors and crystal structures of various Bi_2Te_3-based films deposited on stainless steel substrates.

Bismuth—Fig. 1a shows the cyclic voltammogram obtained with the stainless steel electrodes in 1 M HNO_3 solutions containing 8 mM Bi^{3+}. The scanning directions and starting scanning potentials are also indicated by arrows. Only one couple of reduction/oxidation peaks were observed which are located at −108 and −10 mV (labeled as A and B), respectively. After applying the suitable potentials in the reductive region, the greyish white deposits were formed and single phase of Bi was identified by XRD. Peaks A and B could be associated with the reduction of Bi^{3+} and oxidation of Bi through the following reaction:

$$Bi^{3+} + 3e^- \rightarrow Bi(s) \quad (1)$$

The electrochemical behaviors of Bi on stainless steel electrode were in good agreement with those observed on Pt electrode by Martin-Gonzalez et al.[22] and on Au electrode by Wen et al.[23].

Tellurium—The cyclic voltammogram of stainless steel electrode obtained in 1 M HNO_3 solutions containing 10 mM $HTeO_2^+$ is given in Fig. 1b. It can be seen that a pair of reduction/oxidation peaks appeared at −330 and 490 mV (labeled as C and D), respectively, which is more widely separated as compared with Fig. 1a. After a short limiting current region, hydrogen evolution took place at near −420 mV.

The reductive process of $HTeO_2^+$ may be complicated for tellurium is an amphoteric element. Danaher and Lyons [24] suggested that the deposition mechanism of tellurium is related to the concentration of $HTeO_2^+$: the reaction occurs through a six-electron reduction of $HTeO_2^+$ to H_2Te, followed by a reaction between H_2Te and $HTeO_2^+$ yielding Te. At $HTeO_2^+$ concentrations higher than 1 mM, the second step of this process is very fast and the overall reaction behaves as a four-electron reduction of $HTeO_2^+$ to Te; only at lower $HTeO_2^+$ concentrations (< 1 mM), it was evidently observed for the six-electron reduction. Mori et al. [25] concluded that the reduction occurs through a four-electron reduction of $HTeO_2^+$ to Te(0). However, at more negative potential, on Au substrate, Wen et al. [23] proposed that reduced product Te(0) could be further reduced to H_2Te, and a simultaneous reaction between $HTeO_2^+$ and H_2Te yielded Te(0) on Pt electrode. Martin-Gonzalez et al. [22] suggested another mechanism that $HTeO_2^+$ to H_2Te and simultaneously previously reduced Te(0) at higher potentials to H_2Te, followed by chemical reaction between $HTeO_2^+$ and H_2Te, finally leading to Te(0) as soon as H_2Te is generated electrochemically.

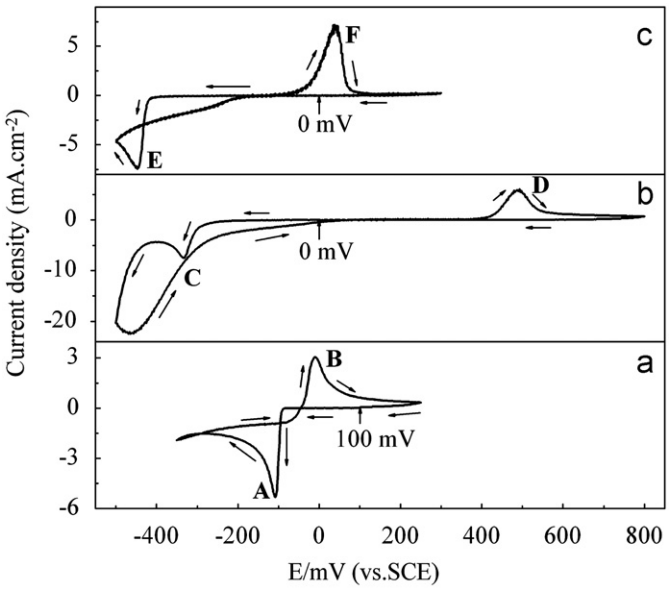

Fig. 1. Cyclic voltammograms of stainless steel electrodes in the solutions containing 1 M HNO_3 and 8 mM Bi^{3+} (a), 10 mM $HTeO_2^+$ (b), 9.75 mM SbO^+ + 0.5 M tartaric acid (c) at 20 mV/s and room temperature.

In our present study, for stainless steel electrode, we observed only one reductive wave in cathodic scanning, therefore, we assigned peak C for the four-electron reduction of $HTeO_2^+$ to Te(0) based on the previous results [17] as given below:

$$HTeO_2^+ + 3H^+ + 4e^- \rightarrow Te(s) + 2H_2O \quad (2)$$

Peak D is due to tellurium dissolution.

Antimony—Fig. 1c is the cyclic voltammogram of stainless steel electrode in solution containing 1 M HNO_3, 9.75 mM Sb(III) and 0.5 M tartaric acid. Similarly, a couple of reduction/oxidation peaks were observed at −430 and 10 mV, respectively (labeled as E and F).

Cotton [26] suggested that Sb_2O_3 was directly dissolved into acid solution (pH ≈ 0–1) and its existence form was SbO^+ with the limited solubility of Sb_2O_3 (about 0.05 mM)[27]. Kotrly and Sucha [28] added tartaric acid as the complexing reagent in solution, leading to the transformation of the existence form of Sb(III) from SbO^+ to a more stable complex ions $[Sb_2(C_4H_4O_6)_2]^{2+}$, therefore, the solubility of Sb_2O_3 was remarkably increased. Li et al. [29] proposed that electrochemical reduction of the complex ion $[Sb_2(C_4H_4O_6)_2]^{2+}$ is much more difficult than that of the ion SbO^+. Hence, the cathodic peak E can be described as the following reaction according to Li et al. [29]:

$$[Sb_2(C_4H_4O_6)_2]^{2+} + 6e^- \rightarrow 2Sb(s) + 2C_4H_4O_6^{2-} \quad (3)$$

Peak F corresponded to the stripping of deposit Sb(0) from the stainless steel.

Bismuth–tellurium—Fig. 2a shows the cyclic voltammogram of stainless steel electrode obtained in solutions containing 1 M HNO_3, 8 mM Bi^{3+} and 10 mM $HTeO_2^+$ (Bi–Te binary system). There were only a pair of reduction/oxidation peaks located at −60 and 470 mV (labeled as G and H), respectively, which indicates one step reduction mechanism for the deposition of Bi_2Te_3.

Takahashi et al. [7] proposed the deposition mechanism of bismuth telluride on Ti substrate: first, the ions diffused from the bulk electrolyte to the electrode surface by the electric field force, and were adsorbed on the substrate. Second, the adsorbed ions were then reduced to Bi(0) and Te(0) at the cathode, respectively. Third, the elemental Te reacted with Bi to form bismuth telluride. Golia et al. [30] and Jin et al.[31] confirmed the same deposit step on conducting glass and Au substrates, respectively. However, Miyazaki and Kajitani [18] put forward another mechanism on Ti sheet: first, metallic Te(0) was reduced from $HTeO_2^+$, and then BiO^+ received electrons on the Te(0) precipitates to form Bi_2Te_3 alloy. On Au substrate, this deposition process was also supported by Li et al. [32].

A recent study by Li et al. [33] has suggested that the deposition mechanism of Bi_2Te_3 on Cu substrate is dependent on the potentials: at potentials higher than −0.1 V(vs. SCE), Bi^{3+} could not be electrochemically reduced on the cathode, but the

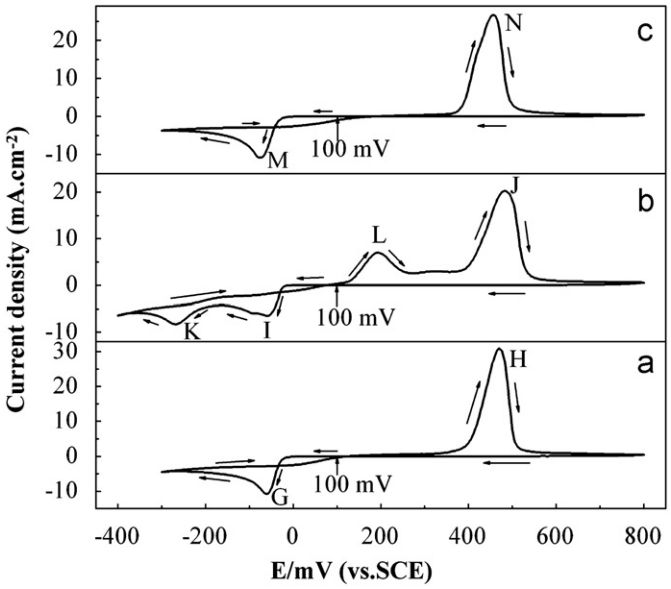

Fig. 2. Cyclic voltamograms of stainless-steel electrodes in solutions containing 1 M HNO_3, 8 mM Bi^{3+}+10 mM $HTeO_2^+$ (a), 2.6 mM Bi^{3+}+10.4 mM SbO^++10 mM $HTeO_2^+$+0.5 M tartaric acid (b), 8 mM Bi^{3+}+9 mM $HTeO_2^+$+1 mM H_2SeO_3 (c), at 20 mV/s and room temperature.

electrochemical reduction of $HTeO_2^+$ to Te^{2-}, then resulted in the precipitation of Bi_2Te_3 on the electrode surface; at potentials lower than −0.4 V (vs. SCE), the process agreed with that described by Takahashi et al. [7].

On stainless steel substrate, the reductive peak G ($E_{pc}=-60$ mV) in solutions containing $HTeO_2^+$ and Bi^{3+} is more positive compared with the reduction of solutions containing only $HTeO_2^+$ ($E_{pc}=-330$ mV) or only Bi^{3+} ($E_{pc}=-108$ mV) for comparable concentrations. This behavior was due to the formation of a compound on the surface of the electrode, which shifts the potentials [22]. This process may be attributed to mutually induced deposition mechanism [34] or pure underpotential deposition (UPD). Applying potentials in the reductive region, the deposits form on the working electrode, which have been proved to be Bi_2Te_3 by XRD, while elemental Bi and Te were not detected in XRD patterns. Therefore, peak G could be assigned to the reduction reactions of $HTeO_2^+$ and Bi^{3+} to Bi_2Te_3 according to

$$HTeO_2^+ + 3H^+ + 4e^- \rightarrow Te(s) + 2H_2O \quad (4)$$

$$3Te(s) + 2Bi^{3+} + 6e^- \rightarrow Bi_2Te_3 \quad (5)$$

The overall reaction became [17]

$$2Bi^{3+} + 3HTeO_2^+ + 9H^+ + 18e^- \rightarrow Bi_2Te_3(s) + 6H_2O \quad (6)$$

There was only one deposit, peak H corresponded to the dissolution of bismuth telluride, which is consistent with Magri et al. [35].

Bi–Sb–Te ternary system—The cyclic voltammograms of single ions revealed that the reductions of Bi^{3+} and $HTeO_2^+$ are much easier than that of SbO^+ in nitric acid system. In order to obtain the stoichiometry of the expected $Bi_{0.5}Sb_{1.5}Te_3$ thin films, the concentration proportion of the three ions in the ternary solution was determined to be $[C(Bi^{3+})+C(SbO^+)]:C(HTeO_2^+) = 13:10 > 2:3$, $C(SbO^+):C(Bi^{3+}) = 4:1 < 3:1$.

The cyclic voltammogram of stainless steel electrode in nitric acid solutions containing 2.6 mM Bi^{3+}, 10.4 mM SbO^+, 10 mM $HTeO_2^+$ and 0.5 M tartaric acid (Bi–Sb–Te ternary system) is shown in Fig. 2b. Two obvious reductive peaks occurred around −60 and −270 mV (labeled as I and K), respectively, in cathodic process, and two oxidation peaks were observed around 190 and 470 mV (labeled as L and J), respectively, in reversal scanning process. It indicates two different mechanisms for the deposition of $Bi_{2-x}Sb_xTe_3$. The CV behaviors are consistent with the previous results of Wang et al. [16]

The potential of peak I was equal to that of peak G in solutions containing Bi^{3+} and $HTeO_2^+$. Applying potentials in the first reductive region, the deposits formed on the working electrode, which have been proved to be single phase solid solution $Bi_{2-x}Sb_xTe_3$ by XRD. Therefore, the reductive peak I of the Bi–Sb–Te ternary system followed the same deposition mechanism as that of Bi–Te binary system. The reductive reactions can be described as

$$HTeO_2^+ + 3H^+ + 4e^- \rightarrow Te(s) + 2H_2O \quad (7)$$

$$3Te(s) + (2-x)Bi^{3+} + xSbO^+ + 6e^- + 2xH^+ \rightarrow Bi_{2-x}Sb_xTe_3 + xH_2O \quad (8)$$

The overall reaction then became [12]

$$3HTeO_2^+ + (2-x)Bi^{3+} + xSbO^+ + (9+2x)H^+ + 18e^- \rightarrow Bi_{2-x}Sb_xTe_3 + (6+x)H_2O \quad (9)$$

At more negative potentials, the Sb(III) changed from simple ions SbO^+ to complex ions $[Sb_2(C_4H_4O_6)_2]^{2+}$, peak K was assigned for the reduction of $[Sb_2(C_4H_4O_6)_2]^{2+}$ to Sb. Comparable to antimony deposition alone, the more positive potential of peak K may contribute to effect of the deposits that form at the first reductive region.

In the anodic scanning process, the potential of peak J was similar to that of peak H in solutions containing Bi^{3+} and $HTeO_2^+$. Peak J corresponded for the dissolution of $Bi_{2-x}Sb_xTe_3$.

The small peak L represents a minor oxidation step. In the binary Bi–Te system, Martin-Gonzalez et al. [22] found that the reductive region is associated with the oxidation of Bi which is the top layer on Bi_2Te_3 film. In unary system, the oxidative peak of elemental Bi is close to that of elemental Sb. Thus, it is considered that peak L was associated with the oxidation of Sb, which is confirmed by the later EPMA analysis (Table 2).

Bi–Te–Se ternary system—Fig. 2c shows the cyclic voltammogram for the solutions containing 1 M HNO_3, 8 mM Bi^{3+}, 9 mM $HTeO_2^+$ and 1 mM H_2SeO_3 (Bi–Te–Se ternary system). It can be seen that only one couple of reduction/oxidation peaks (labeled as M and N) located at −73 and 465 mV, respectively. It indicates only a single mechanism for the deposition of $Bi_2Te_{3-y}Se_y$.

The potential of peak M was quite similar to that of peak G in solutions containing Bi^{3+} and $HTeO_2^+$. The deposit formed on the working electrode when applying potentials in the reductive region, which is in a single phase solid solution $Bi_2Te_{3-y}Se_y$ confirmed by XRD. Therefore, a similar deposition mechanism existed between the Bi–Te–Se system and Bi–Te system. The reductive peak M was caused due to the reduction of Bi^{3+}, $HTeO_2^+$ and H_2SeO_3 to $Bi_2Te_{3-y}Se_y$.

The process can be described as following steps: first, the Bi^{3+}, $HTeO_2^+$ and H_2SeO_3 from bulk electrolyte diffused to the stainless steel electrode surface and adsorbed on the surface by the electric field force; then, the ions can mutually induced codeposition by the following reactions:

$$HTeO_2^+ + 3H^+ + 4e^- \rightarrow Te(s) + 2H_2O \quad (10)$$

$$H_2SeO_3 + 4H^+ + 4e^- \rightarrow Se(s) + 3H_2O \quad (11)$$

$$(3-y)Te(s) + ySe(s) + 2Bi^{3+} + 6e^- \rightarrow Bi_2Te_{3-y}Se_y(s) \quad (12)$$

The overall reaction could be described as the following reaction [13]:

$$2Bi^{3+} + (3-y)HTeO_2^{+} + (y)H_2SeO_3 + (9+y)H^{+} + 18e^{-} \rightarrow Bi_2Te_{3-y}Se_y + (6+y)H_2O \quad (13)$$

There was only one deposit, peak N corresponded for the dissolution of $Bi_2Te_{3-y}Se_y$.

3.2. Film deposition and characterization

The composition of the deposits—Table 1 shows the compositions of the Bi–Te films obtained at different deposition potentials between −25 and −250 mV in the Bi–Te binary system. For all the films, the Bi:Te atomic percentage ratio was almost 2:3, which indicates that the composition of the films was not strongly dependent on the deposition potentials in the reductive region obtained by CV.

Table 2 lists the compositions of the Bi–Sb–Te films as a function of the deposition potential in the Bi–Sb–Te ternary system. The contents of Sb and Te in the Bi–Sb–Te films were remarkably changed by varying the deposition potentials from −80 to −200 mV. With negative shift of the potentials, the Sb content increased while the Te content decreased, which agreed well with the CV in Fig. 2(b). Those results can be attributed to more negative reductive potential of SbO^{+}/Sb than that of the $HTeO_2^{+}$/Te system. The composition of the films was maintaining relatively steady at the deposition potentials between −200 and −350 mV which is corresponding to the range of the second reductive region obtained by CV.

Table 3 shows the compositions of the Bi–Te–Se films as a function of the deposition potential in the Bi–Te–Se ternary system. For the potentials ranging between 25 and −25 mV, the stoichiometry remained stable. More negative deposition potential caused a slight increase of Bi content and small decreases of Te and Se.

Table 1
The compositions of the films deposit at various cathodic potentials in solutions containing 1 M HNO3, 8 mM Bi^{3+} and 10 mM $HTeO_2^{+}$.

E/mV (vs. SCE)	Composition (atomic%)	
	Bi	Te
−25	40.24	59.76
−50	40.16	59.84
−75	39.01	60.99
−100	39.88	60.12
−150	40.46	59.54
−200	39.74	60.26
−250	39.50	60.50

Table 2
The compositions of the films deposit at various cathodic potentials in solutions containing 1 M HNO_3, 2.6 mM Bi^{3+}, 10.4 mM SbO^{+}, 10 mM $HTeO_2^{+}$ and 0.5 M tartaric acid.

E/mV (vs. SCE)	Composition (atomic%)		
	Bi	Sb	Te
−80	13.96	22.70	63.54
−120	11.92	27.93	60.15
−150	12.84	29.77	57.39
−200	12.13	39.66	48.21
−250	12.69	37.87	49.44
−300	11.88	36.58	51.55
−350	11.78	39.61	48.61

Table 3
The compositions of the films deposit at various cathodic potentials in solutions containing 1 M HNO_3, 8 mM Bi^{3+}, 9 mM $HTeO_2^{+}$ and 1 mM H_2SeO_3.

E/mV (vs. SCE)	Composition (atomic%)		
	Bi	Te	Se
25	40.23	54.40	5.37
0	40.28	53.71	6.01
−25	40.35	53.27	6.39
−50	41.63	53.01	5.35
−75	42.55	52.71	4.73
−100	42.03	52.98	4.99
−150	41.55	51.94	6.51

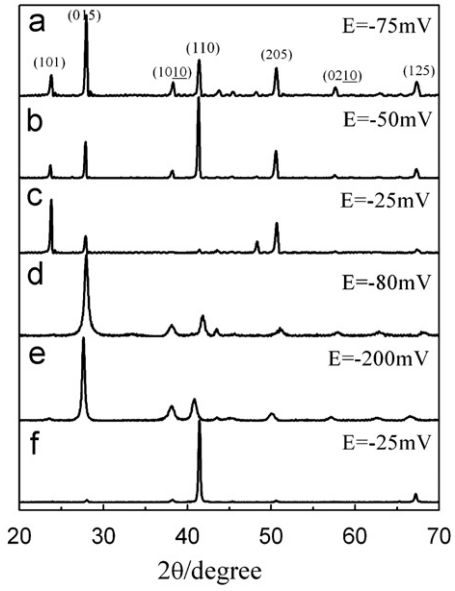

Fig. 3. XRD patterns of the films deposited at various cathodic potentials in solutions containing 1 M HNO_3, 8 mM Bi^{3+}+$HTeO_2^{+}$ (a) (b), 2.6 mM Bi^{3+}+10.4 mM SbO^{+}+10 mM $HTeO_2^{+}$+0.5 M tartaric acid (c), 8 mM Bi^{3+}+9 mM $HTeO_2^{+}$+1 mM H_2SeO_3 (d) (e) (f).

X-ray diffraction identification—XRD patterns of deposits obtained at various potentials in different solutions are shown in Fig. 3. We can see that all the films were single phase within the deposition potential ranges. All of the detected peaks corresponded to ICDD powder diffraction file for Bi_2Te_3 with a rhombohedral crystal structure. It revealed that Sb and Se elements are doped into bismuth telluride. The Bi_2Te_3 showed a strong (1 1 0) preferred orientation at higher potentials (Fig. 3a) and (0 1 5) orientation at potentials below −200 mV (Fig. 3b). The Sb-doped bismuth telluride thin films showed strong (1 0 5) preferred orientation within the deposition potential range (Fig. 3c). While the Se-doped bismuth telluride thin films showed different preferred orientations (Fig. 3d-f) at various potentials.

ESEM observations—Fig. 4 illustrates the morphologies of the films at various deposition potentials in different systems. The undoped Bi_2Te_3 thin films exhibited metallic luster and homogeneous grains (Fig. 4a) deposited at higher potentials, while the films showed dendritic structure (Fig. 4b) at lower potentials. The Sb-doped (Fig. 4c, d) and Se-doped (Fig. 4e, f) bismuth telluride thin films were black and gray, respectively.

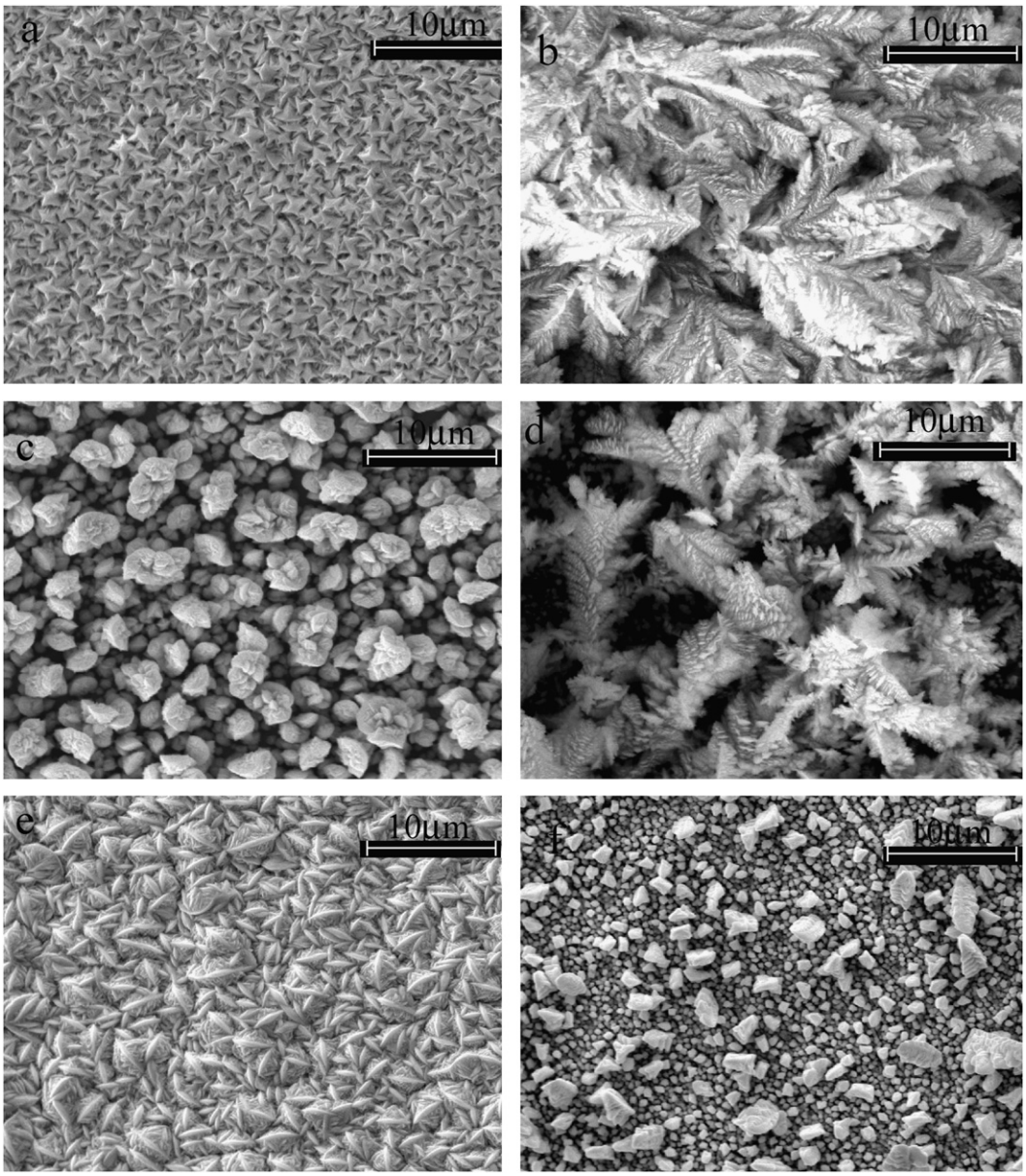

Fig. 4. SEM images of films deposited at various cathodic potentials in solutions containing 1 M HNO_3, 8 mM Bi^{3+} +1 mM $HTeO_2^+$ (a) −25 mV (b) −200 mV, 2.6 mM Bi^{3+} +10.4 mM SbO^+ +10 mM $HTeO_2^+$ +0.5 M tartaric acid (c) −150 mV (d) −300 mV, 8 mM Bi^{3+} +9 mM $HTeO_2^+$ +1 mM H_2SeO_3 (e) −25 mV and (f) −150 mV.

With negative shift of the deposition potentials, all of them became crude and inhomogeneous. Therefore, the morphology of the films was tremendously dependent on the potentials.

4. Conclusions

In this work, we systematically studied the electrochemical reduction processes of Bi_2Te_3, p-type $Bi_{0.5}Sb_{1.5}Te_3$ and n-type $Bi_2Te_{2.7}Se_{0.3}$ compounds. At higher potentials, they had the similar deposition mechanism: first, the quadrivalence $HTeO_2^+$ or H_2SeO_3 was reduced to Te(0) or Se(0), respectively. Second, Bi^{3+} received electrons on Te to form Bi_2Te_3 (Bi–Te binary system); Bi^{3+} received electrons on Te and Se to form $Bi_2Te_{2.7}Se_{0.3}$ alloys (Bi–Te–Se ternary system); Bi^{3+} and SbO^+ received electrons on the Te precipitates to form $Bi_{0.5}Sb_{1.5}Te_3$ alloys (Bi–Sb–Te ternary system). The films having stoichiometry of Bi_2Te_3, $Bi_{0.5}Sb_{1.5}Te_3$ and $Bi_2Te_{2.7}Se_{0.3}$ were single phase with the rhombohedral Bi_2Te_3 structure. Morphology and crystal orientation of the films were dependent on the deposition potentials. At higher potentials, they became homogeneous and smooth.

Acknowledgements

This work was supported by the National Natural Science Foundation of China (50532010) and Fujian Key Laboratory of Advanced Materials, China, (2006L2003).

References

[1] I.-H. Kim, Mater. Lett. 43 (2000) 221.
[2] J.P. Fleurial; A. Borshchevsky; M. Ryan; W. Phillips; J. Snyder; T. Caillat; E. Kolawa; J. Herman; P. Mueller; M. Nicolet, Mater. Res. Soc. Symp. Proc., 545 (1998) 493.
[3] R.G. Cope, A.W. Penn, J. Mater. Sci. 3 (1968) 103.
[4] J. Jiang, L. Chen, S. Bai, Q. Yao, Q. Wang, J. Cryst. Growth 277 (2005) 258.

[5] A. Giani, F. Pascal-Delannoy, A. Boyer, A. Foucaran, M. Gschwind, P. Ancey, Thin Solid Films 303 (1997) 1.
[6] A. Boulouz, A. Giani, F. Pascal-Delannoy, M. Boulouz, A. Foucaran, A. Boyer, J. Cryst. Growth 194 (1998) 336.
[7] M. Takahashi, Y. Oda, T. Ogino, S. Furuta, J. Electrochem. Soc. 140 (1993) 2550.
[8] S.H. Li, M.S. Toprak, H.M.A. Soliman, J. Zhou, M. Muhammed, D. Platzek, E. Muller, Chem. Mater. 18 (2006) 3627.
[9] P. Heo, K. Hagiwara, R. Ichino, M. Okido, J. Electrochem. Soc. 153 (2006) C213.
[10] D. Del Frari, S. Diliberto, N. Stein, C. Boulanger, J.M. Lecuire, Thin Solid Films 483 (2005) 44.
[11] F.H. Li, Q.H. Huang, W. Wang, Electrochim. Acta 54 (2009) 3745.
[12] Q. Huang, W. Wang, F. Jia, Z. Zhang, J. Univ. Sci. Technol. Beijing, Mineral, Metall., Mater. 13 (2006) 277.
[13] M. Martin-Gonzalez, G.J. Snyder, A.L. Prieto, R. Gronsky, T. Sands, A.M. Stacy, Nano Lett. 3 (2003) 973.
[14] H. Kose, M. Bicer, G. Tutuoglu, A.O. AydIn, I. Sisman, Electrochim. Acta , doi:10.1016/j.electacta.2008.09.059.
[15] S. Michel, S. Diliberto, N. Stein, B. Bolle, C. Boulanger, J. Solid State Electrochem. 12 (2008) 95.
[16] W. Wang, G.Q. Zhang, X.G. Li, J. Phys. Chem. C 112 (2008) 15190.
[17] P. Magri, C. Boulanger, J.M. Lecuire, J. Mater. Chem. 6 (1996) 773.
[18] Y. Miyazaki, T. Kajitani, J. Cryst. Growth 229 (2001) 542.
[19] J. Zhou, S. Li, H.M.A. Soliman, M.S. Toprak, M. Muhammed, D. Platzek, E. Muller, Phys. Status Solidi (c) 5 (2008) 3453.
[20] S. Li, H.M.A. Soliman, J. Zhou, M.S. Toprak, M. Muhammed, D. Platzek, P. Ziolkowski, E. Muller, Chem. Mater. 20 (2008) 4403.
[21] L. Bu, W. Wang, H. Wang, Appl. Surf. Sci. 253 (2007) 3360.
[22] M. Martin-Gonzalez, A.L. Prieto, R. Gronsky, T. Sands, A.M. Stacy, J. Electrochem. Soc. 149 (2002) C546.
[23] S. Wen, R.R. Corderman, F. Seker, A.P. Zhang, L. Denault, M.L. Blohm, J. Electrochem. Soc. 153 (2006) C595.
[24] W.J. Danaher, L.E. Lyons, Aust. J. Chem. 36 (1984) 1011.
[25] E. Mori, C.K. Baker, J.R. Reynolds, K. Rajeshwar, J. Electroanal. Chemistry and Interfacial Electrochem. 252 (1988) 441.
[26] F.A. Cotton, in: Adv. Inorg. Chem., Interscience Publishers, New York, 1972.
[27] G. Jung, C.K. Rhee, J. Electroanal. Chem. 436 (1997) 277.
[28] S. Kotrly, L. Sucha, in: Handbook of chemical equilibria in analytical chemistry, E. Horwood, Halsted, New York, 1985.
[29] F.H. Li, W. Wang, J.P. Gao, S.Y. Wang, J. Electrochem. Soc. 156 (2009) D84.
[30] S. Golia, M. Arora, R.K. Sharma, A.C. Rastogi, Curr. Appl. Phys. 3 (2003) 195.
[31] C.G. Jin, X.Q. Xiang, C. Jia, W.F. Liu, W.L. Cai, L.Z. Yao, X.G. Li, J. Phys. Chem. B 108 (2004) 1844.
[32] F.H. Li, F.L. Jia, W. Wang, Appl. Surf. Sci. 255 (2009) 7394.
[33] G.R. Li, F.L. Zheng, Y.X. Tong, Cryst. Growth Des. 8 (2008) 1226.
[34] F.A. Kroer, J. Electrochem. Soc. 125 (1978) 2028.
[35] P. Magri, C. Boulanger, J.M. Lecuire, AIP Conf. Proc., 316 (1994) 277.